AIAA Propulsion and Energy Forum
19-22 August 2019, Indianapolis, IN
AIAA Propulsion and Energy 2019 Forum

10.2514/6.2019-4447

Small-volume, High-throughput Techniques for Fuel Physical Property Measurements

Wanjun Dang*, Shyam Menon†
Louisiana State University, Baton Rouge, LA, 70808

Fuel physical properties including surface tension, viscosity play a key role in spray atomization and mixing processes in IC engines affecting their combustion and emission characteristics. The ongoing development of a small-volume, high-throughput screening tool for fuels has required the development of techniques to utilize minute fuel quantities, of the order of 5 µL, and provide information on relevant physical properties in a rapid fashion. To this end, the shape oscillation dynamics of single droplets generated by a piezo-electric device are used to measure surface tension and viscosity. The measurement techniques are applied to primary reference fuels (Isooctane and N-heptane) as well as relevant bio-fuels such as 2-butanone, butyl acetate, and others. Results for surface tension and viscosity are correlated with literature data as well as data obtained using standard reference instruments. Overall, the objective of this work is to demonstrate the validity of the techniques used to measure fuel physical properties in a rapid manner using a limited sample size.

I. Introduction

Increasingly there is a desire to incorporate more renewable fuel sources in aerospace applications. There have been efforts to investigate the potential benefits of biofuels in both military and civilian aircraft applications [1]. Previous work has also focused on evaluation of performance and emission benefits by using biofuels in gas turbine engines [2] [3]. While several of these previous efforts have focused on engine-level performance, it is also important to evaluate other significant effects of using biofuels as drop-in replacements for aviation fuels in gas turbine engines that might have an underlying influence on engine performance. Fuel injection, atomization, vaporization, and mixing play key roles in the subsequent combustion of the fuel-air mixture. Biofuels can have significantly different physical properties as compared to conventional aircraft fuels. This can result in key differences in several of the physical processes listed above resulting in a change in engine performance and emissions. An increase in fuel viscosity can delay spray breakup due to dampening of surface disturbances on the liquid jet. Increased surface tension results in higher cohesive forces making the generation of smaller droplets through secondary atomization more difficult [4].

However, a significant hurdle is that there are many hundreds of kinds of biofuels that can potentially be produced [5] [6]. It is not feasible to pursue a development approach where each of these fuel varieties can be subjected to a complete test program by utilizing it in an engine and measuring engine performance and emissions over a range of operating conditions. To this end, a screening tool is desired that can rapidly screen potential candidate fuels and provide information regarding key physical properties like surface tension, viscosity, and heat of vaporization as well as combustion metrics such as flame speed and ignition delay which influence the performance of the fuel when used in an engine. Further, the screening tool should have the ability to work with small quantities of fuel (micro-liters), which may be produced for evaluation purposes.

This work describes ongoing efforts to measure physical properties of biofuels using droplet dynamics. A

* Graduate Research Assistant, Mechanical and Industrial Engineering Department, wdang3@lsu.edu
† Assistant Professor, Mechanical and Industrial Engineering Department, smenon@lsu.edu

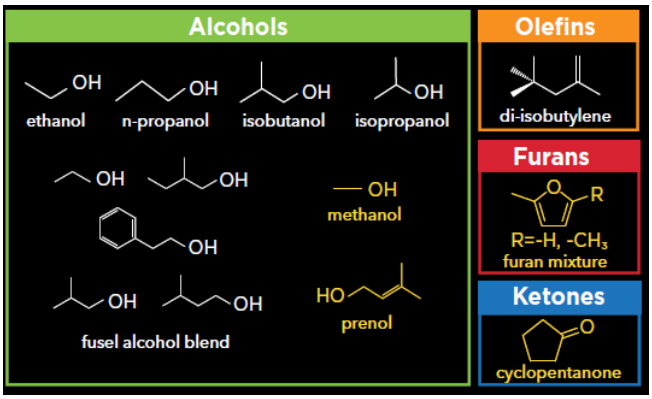

Figure. 1 Blendstocks with highest merit function scores [7].

piezoelectric droplet generator is used to produce a continuous train of droplets with size ranging from 30-70 µm. The oscillation dynamics of the droplets are captured in flight using a stroboscopic imaging technique. Image analysis and post-processing are used to estimate the decay rate and frequency of the oscillation, required to calculate fuel surface tension and viscosity. Measurements are carried out for four biomass-derived functional molecules of interest [8] as well as two primary reference fuels. Measurement results are compared with literature data. Additionally, standard reference tests for surface tension and viscosity are carried out using a tensiometer and a viscometer.

The results are compared to evaluate the ability of the droplet generation technique to determine fuel properties using minute quantities of fuel.

II. Theory

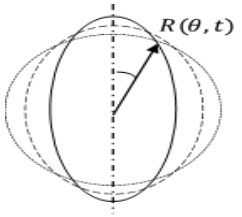

Figure. 2 Sketch showing the variation of the droplet radius as a function of time and polar angle due to droplet oscillation.

The study of droplet oscillation during free fall is of interest in this work because both surface tension and viscosity values can be calculated from damped oscillation frequency and amplitude. Once a droplet pinches off from the nozzle orifice, the process of droplet deformation and restoration looks like the response of a damped oscillator. Surface tension acts as a restoring force to maintain the mechanical equilibrium of the droplet after applying external perturbation. The damping rate of droplet shape oscillation is closely related to viscosity. For an isolated liquid drop undergoing small amplitude axisymmetric oscillation, the droplet shape R(θ,t) as Figure. 2 shows, can be described by [9] [11],

$$R(\theta,t) = R_0 + \xi = R_0 + S_n \cdot \sin(w_n t + \varepsilon) = R_0 + \sum_{n=2}^{\infty} A_n(t) P_n(cos\theta) \qquad (1)$$

where θ is the polar angle, R_0 is the initial radius of a spherical droplet at equilibrium free from other forces except surface tension, ξ is the surface deformation, S_n is a surface-harmonic of order n, which consists of Legendre polynomials P_n, w_n is the oscillation frequency of the nth mode, and ε is the phase shift, and $A_n(t)$ is the surface mode amplitude coefficients.

At $R = R_0$, the surface deformation ξ can be related with velocity potentials as following:

$$\frac{\partial \xi}{\partial t} = -\frac{\partial \phi_l}{\partial R} = -\frac{\partial \phi_g}{\partial R} \quad (2)$$

For an inviscid droplet, the velocity potentials for the droplet and its external medium are:

$$\varphi_l = -\frac{w_n R_0}{n}\left(\frac{R}{R_0}\right)^n S_n \cos(w_n t + \varepsilon) \quad (3)$$

$$\varphi_g = \frac{w_n R_0}{n+1}\left(\frac{R_0}{R}\right)^{n+1} S_n \cos(w_n t + \varepsilon) \quad (4)$$

The oscillation frequency of the n[th] mode w_n is:

$$w_n^2 = (2\pi f_n)^2 = \frac{n(n-1)(n+1)(n+2)\sigma}{R_0^3[(n+1)\rho_f + n\rho_a]} \quad (5)$$

where ρ_f is the density of droplet, ρ_a is the density of ambient air, n is the number of oscillation mode, and σ is the surface tension of the droplet.

Lamb [10] expressed the generalized linear solution for a free oscillating droplet with small amplitude including the influence of the surrounding medium. The viscous effects are introduced by Lamb who provided the following decay time constant τ :

In Equation (1), $A_n(t) \propto e^{-\frac{t}{\tau}}$, where $\tau = \frac{1}{(n-1)(2n+1)}\frac{\rho_f R_0^2}{\mu}$ (6)

where μ is the dynamic viscosity of the droplet.

By measuring the decay time constant τ and the oscillation frequency ω_n, viscosity and surface tension can be estimated after substituting the fluid and ambient densities into Equation (5) and (6).

III. Experiment

3.a Setup

3.a.1 Droplet generator setup

Figure. 3 shows details of the major components of the experimental setup used to obtain measurements of surface tension and viscosity by oscillation dynamics. A continuous train of fuel droplets with specified frequency is generated using a piezoelectric droplet generator made by MicroFab Inc. Figure. 4 shows a photo of the piezoelectric device. When the droplet generator senses an external voltage pulse from the signal generator (Microfab JetDrive V (CT-M5-01)), as shown in Figure. 5, the piezoelectric actuator expands or contracts according to the polarity of the waveform. This fast deformation results in droplet formation at nozzle tip once the equilibrium condition is reached at the meniscus of the 30μm nozzle orifice. The pressure controller (MicroFab CT-PT-21) is used to provide stable back pressure to sustain a balanced force at the liquid meniscus formed at the nozzle orifice. The pressure controller is connected to a vacuum pump as well as a compressed air source (Ultra-pure carrier grade air) allowing it to maintain positive or negative backpressure so that the equilibrium condition can be reached at the meniscus. The test cases in this paper cover a range of backpressures between -0.4 inHg to -0.1 inHg, droplet sizes between 30-45 μm in diameter, and initial velocity around 1m/s. Droplet size and initial velocity can be controlled using the amplitude and shape of the waveform applied to the piezoelectric actuator. The frequency of the pulse controls the droplet spacing. A 2.35 MP CMOS camera (IDS UI-3060CP Rev. 2) mounted on a vertical traverse is used to obtain real-time images of the droplets. A telecentric lens (6X, 65mm WD CompactTL™ Telecentric Lens) made by Edmund Optics having a resolution of 0.97 $\mu m/pixel$, providing detailed images of the droplet. An LED strobe (VLCS5830 Vishay) located on the opposite side of the lens and mounted on another vertical traverse is the light source for the camera.

A hardware triggered setup using a National Instruments myRio data acquisition and control unit is used to synchronize the signals and acquire images. The timing diagram for the myRio is plotted in Figure. 6.

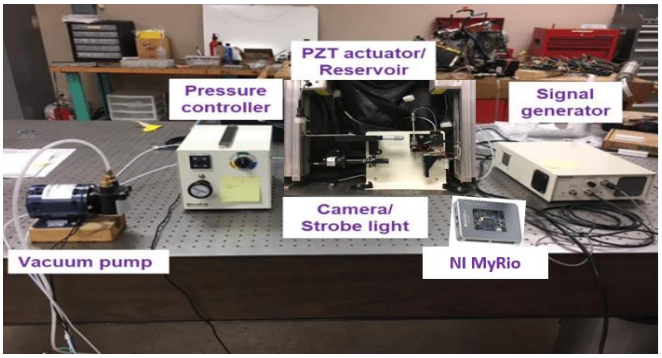

Figure. 3 Major experimental setup for evaluation of surface tension and viscosity using the droplet generator.

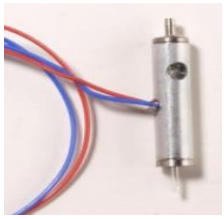

Figure. 4 **Microfab piezoelectric droplet generator [12].**

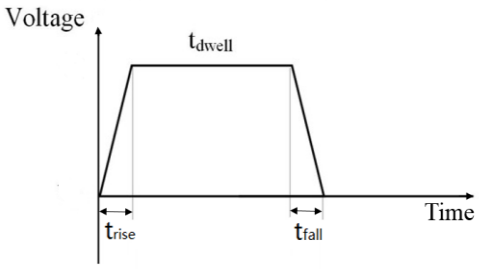

Figure. 5 **Waveform applied to piezoelectric droplet generator.**

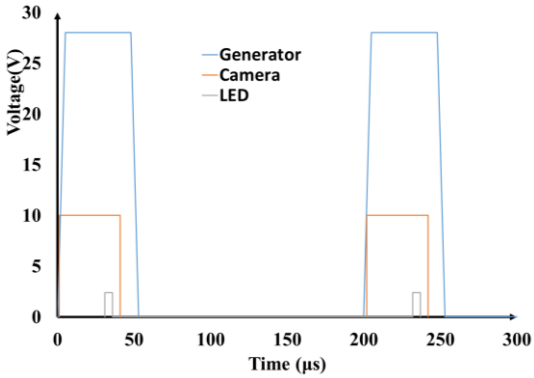

Figure. 6 Timing diagram regarding myRio output pulses to camera/LED and droplet generator.

The generator signal refers to the voltage pulse supplied to the piezoelectric device while the camera and LED signals refer to their trigger signals. While the signal generator produces the voltage waveform for the droplet generator, the camera and LED trigger signals are generated by the myRio device. A fixed time delay of 30 μs for biofuels and 26 μs for isooctane and N-heptane separates the start of the camera trigger from the start of the LED trigger. This ensures that the camera sensor is fully operational and recording by the time the LED is triggered and thus overcomes the latency (below 100 μs) of the camera. The camera trigger signal itself is separated from the generator pulse by a value which changes for each captured image. The delay value is incremented by a fixed amount (1 μs for most cases) in each cycle. This provides the stroboscopic imaging required to generate a time series of droplet images for post-processing. The hardware triggered setup was developed due to the fact that initial tests showed the supplier provided imaging technique to be unsuitable for this work due to several reasons. One, the timing was software controlled and subject to latency issues. This resulted in the background lighting being inconsistent from one image to another. Two, successive images could be obtained with a minimum time separation of 1 μs, while lower values are desired for measurement with fluids having a higher viscosity. The current setup ensures a single LED flash for each image and the timing is tuned to ensure that only a single droplet is present in each image. The images obtained by hardware triggering have consistent background, eliminating the variation in background intensity and improving the accuracy with which the droplet edge is detected. Figure. 7 shows the oscillation process without hardware triggering with non-uniform background light intensity. Figure. 8 shows images captured using hardware triggering resulting in a uniform background light intensity.

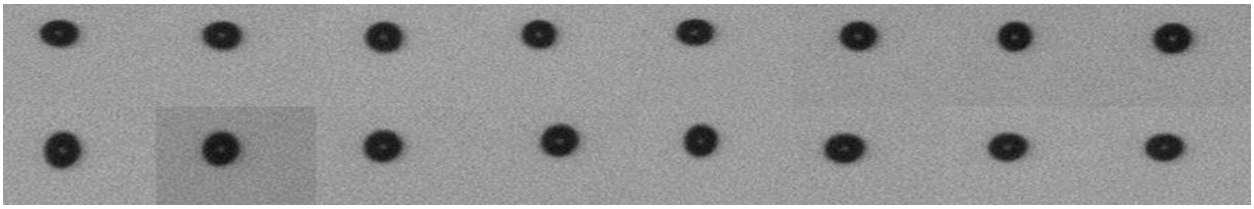

Figure. 7 A sequence of images obtained using strobed imaging showing the oscillation of a 40 µm sized Butyl Acetate droplet without hardware trigger.

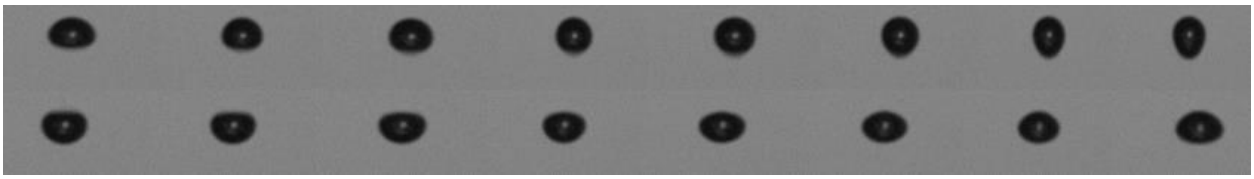

Figure. 8 A sequence of images obtained using strobed imaging showing the oscillation of a 40 µm sized Butyl Acetate droplet with hardware trigger.

3.a.2 Reference measurements

The instruments shown in Figure. 9 including a tensiometer (Attension Theta by Biolin Scientific) and viscometer (Cannon Fenske Routine Viscometer) were used to evaluate the surface tension and viscosity of fuels for comparison with literature data as well as results obtained using the droplet oscillation dynamics. The minimum sample volume required for surface tension and viscosity measurements are 15mL and 7 mL. And the expected accuracy for the measurements of surface tension and viscosity are 0.1% [13-14].

Figure. 9 Tensiometer [15] and Viscometer [16] for reference measurement.

3.b Measurement procedure

3.b.1 Procedure for droplet generator experiment

Before the measurement, the camera, generator and LED need to be aligned and focused. Next, the meniscus at nozzle orifice is adjusted using the pressure controller to achieve equilibrium. Following this, the JetServer program that controls the droplet generator is used to start the jetting process with the required process parameters. Once stable droplet generation is observed on the live video mode of the camera, the hardware triggered image acquisition is activated. The myRio device triggers the camera to take images which are transmitted over USB to a computer running IDS image recording software. The sequence of strobed images is saved as a video file on the computer. During image processing, individual frames are extracted from the video, following which the frames showing droplet motion are picked for further image processing using MATLAB. This will be elaborated further in Section 3.c.

3.b.2 Measurement steps for reference experiment

For surface tension measurement by optical tensiometer, the shape of a pendant droplet hanging on the needle is recorded by a machine vision camera and analyzed by software to determine the contact angle and surface tension. The solution of Young-Laplace equation by iterative approximation can be used to derive the shape factor of the pendant droplet, which helps to determine the surface tension [15].

For viscosity measurement by glass capillary kinematic viscometer, there are four major steps for the operation procedure. Firstly, the tube with a minimum of 7mL sample is filled by suctioning the sample into the double bulb section. Secondly, the tube is returned to upright position and wiped to be clean. Thirdly, the viscometer is placed into a constant temperature bath to reach equilibrium condition. Finally, the viscosity is calculated by timing the flow between two marks and multiplying the time by a constant of the specific viscometer.

3.c Image processing and calculations

Once the images are obtained, a sequence of processing steps are carried out to determine the droplet radius at a certain polar angle, θ, and its variation with time. These steps are shown in

Figure. 10. Once the droplet radius is obtained as a function of time, Equation (1) is solved using least-squares to obtain the mode amplitude coefficients. Figure. 11 shows a plot of the ratio of the amplitude coefficient for the second mode to the droplet radius at equilibrium condition plotted as a function of time. The next step is to determine the decay rate from this damping curve using curve fits as well as the oscillation frequency by a discrete Fourier transform.

The image post-processing steps are carried out using MATLAB including the following 5 steps as shown in

Figure. 10. Step 1 is image batch cropping, after which the droplet is the only object retained in the series of images. Step 2 is background subtraction. After selecting an image without a droplet as the background, applying the image subtraction command can remove the noise from the background and improve the accuracy of droplet edge detection. Step 3 is edge detection by applying an algorithm to accurately locate the contour of the droplet edges. There are a number of edge detection algorithms available. This work primarily considered 1st gradient based algorithms like Canny, Sobel, Prewitt, and Roberts [17] as well as the partial area effect based subpixel edge detection routine [18]. Prewitt algorithm works best for most of the images obtained in this research. Because Prewitt operator places equal focus on pixel detection in the mask, so the detection performance is better than other gradient based algorithms. When comparing Sobel, Roberts and Prewitt algorithms, as Figure. 12 shows, the gradient is calculated regarding the central pixel with coordinates [i, j]. Roberts operator outputs gradient corresponding to the 45 and 135 degrees edge response, while Sobel and Prewitt operators output horizontal and vertical edge response. Roberts and Sobel operators place emphasis on pixels that are closer to the center of the masks, while Prewitt operator does not have this location preference. So this may explain why Prewitt operator works well in all cases especially when there are minor light intensity differences. Step 4 is centroid determination based on the binary image using a built-in centroid detection function in Matlab. Step 5 is to solve mode amplitude coefficients using least-square curve fitting. Once the zero and second order mode coefficients had worked out, the surface tension and viscosity can be calculated after fitting a decay curve and using Fast Fourier Transform (FFT) to find the decay rate and the oscillation frequency using Equations (5) and (6).

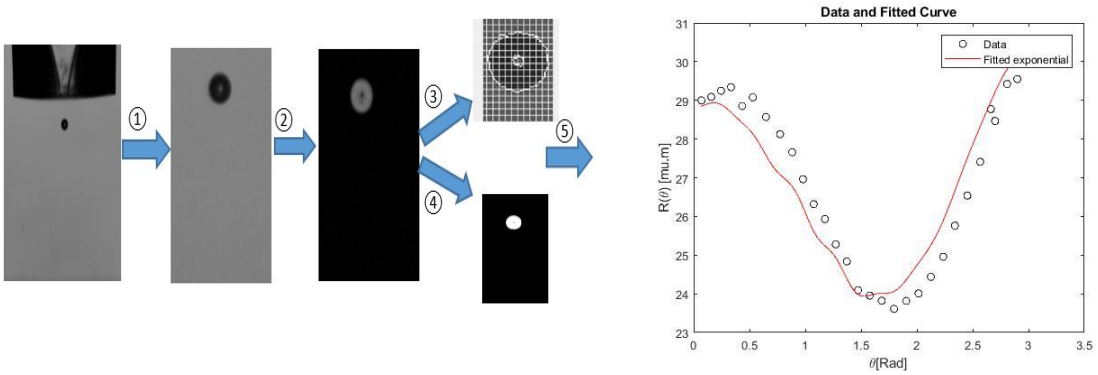

Figure. 10 Image processing steps to obtain the droplet radius at a certain polar angle as a function of time.

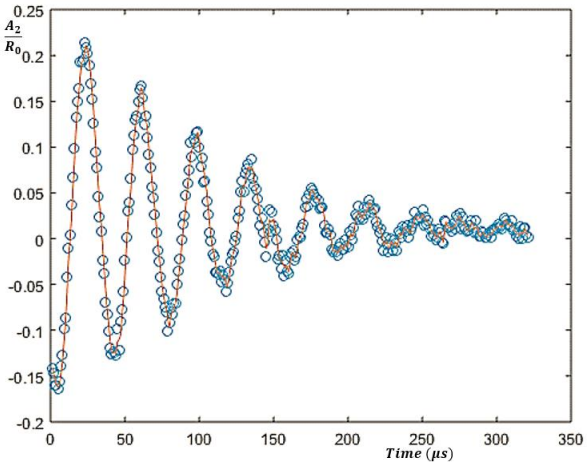

Figure. 11 The ratio of the mode amplitude coefficient to the droplet radius plotted as a function of time.

a_0	a_1	a_2
a_7	[i, j]	a_3
a_6	a_5	a_4

Figure. 12 The labeling of neighboring pixels in a mask.

3.d Fuels tested

Six fuels of interest were tested in this work. This includes *iso*-octane and *n*-heptane which are primary reference fuels. The remaining four fuels are bio-derived functional group fuel molecules deemed to be of interest as a drop-in replacement or blended component for gasoline fuel. Table 1 shows key information regarding the fuels tested in this work at 17 °C, atmospheric pressure condition as well as the settings corresponding to the droplet generator, and the LED used in this work.

Table 1 Jetting parameters set for the various test cases.

	2-Butanone	Butyl Acetate	2,5 Dimethylfuran	1-Butanol	*n*-heptane	*iso*-octane
Voltage (V)	31	28	30	29	29	31
Dwell time (µs)	43	43	38	40	40	40
Rise/fall time (µs)	5	5	5	5	5	5
Frequency (Hz)	300	300	300	300	300	300
Backpressure (inHg)	-0.2	-0.1	-0.2	-0.1	-0.1	-0.4
Strobe on duration (µs)	5	5	5	5	5	5
Strobe delay (µs)	1	1	1	0.5	1	1
Surface Tension from Literature (mN/m)	24.66 [20]	25.73 [19]	25.86 [24]	25.65 [19]	20.43 [19]	21.9 [19] [20]
Surface Tension from Tensiometer (mN/m) [17]	22.60	23.16	24.92	23.30	NA	NA
Viscosity from Literature (mPaS)	0.44 [21]	0.79 [19]	0.55 [22]	2.74 [19]	0.43 [19] [23]	0.56 [23]

IV. Results

4.a Impact of strobe duration

Table 2 Deviation of surface tension and viscosity from reference values with respect to strobe duration for N-heptane.

Strobe on-time duration (μs)	Surface tension (%)	Viscosity (%)
3	-2.81	16.46
4	-2.96	2.68
5	-7.20	5.27
6	-7.41	24.28
7	-11.10	23.12

The duration for which the LED light is turned on has a strong impact on the measurement results. The major impact of the LED on-time duration is due to the fact that the droplets are moving once ejected from the nozzle orifice. The droplets travel with an average velocity of 1-2 m/s. And the image sensor records light primarily when the LED is turned on for 5 μs. During this time the droplet travels a distance of about 5-10 μm. The effect of the strobe duration was evaluated by conducting tests where the only variable was the duration for which the LED was turned on. Table 2 reports the deviation from literature values corresponding to each value of LED on-time duration. Considering the literature data presented in Table 1, the deviation from the literature value is least for a strobe on-time duration of 4 μs and increases with further decreases or increases in on-time duration. The effect of blurring due to droplet motion is likely compounded by increase in signal noise due to potential light scattering by droplet surface waves and surface

motion resulting from droplet motion and oscillation. A strobe on time duration of 5 μs is selected for all the tests conducted in this work, which provides a reasonable balance between having sufficient contrast in the image to detect the droplet edges without incurring too much noise due to scattering or blurring during droplet motion.

4.b Impact of edge detection algorithm

Given the availability of several edge detection algorithms, it was decided to investigate the accuracy of surface tension and viscosity measurement as it relates to the choice of the algorithm. Table 3 shows a comparison between different edge detection algorithms using data for *n*-heptane with a fixed strobe on-time duration of 5 μs. The deviation from the reference value is provided for the different edge detection algorithms. A significant scatter is observed in the measurement values based on the choice of the algorithm. As explained in 3.c, Prewitt operator places equal emphasis of the pixels around the center of mask, so this may explain why Prewitt operator works well in all cases, not only the case shown in Table 3, but also the cases shown in other data series. And Prewitt operator excels especially when there are minor light intensity differences from LED. The subsequent results are analyzed based on Prewitt edge detection method.

Table 3 Deviation of surface tension and viscosity with respect to edge detection method for pure n-heptane at 4μs strobe on time.

Edge Detection Method	Deviation of Surface tension (%)	Deviation of Viscosity (%)
Prewitt	-2.96	2.68
Subpixel	-3.22	33.86
Sobel	4.24	14.56
Canny	6.12	31.83
Roberts	0.83	2.84

4.c Repeatability analysis

The strobed imaging approach used in this work has the key advantage that it is not required to follow a single droplet through its oscillation dynamics using a high-cost high-speed camera. The use of a machine vision camera lends well to this effort since the objective is to develop a low-cost screening tool for biofuels. However, an inherent assumption in this approach is that each successive droplet is generated in exactly the same manner and the oscillation dynamics that follow are exactly repeatable for the successive droplets. To gauge the validity of this assumption, a repeatability analysis was conducted by collecting seven consecutive data sets for each of the fuels tested in this work. The results of this repeatability analysis are now presented for 2-butanone. The droplet generator settings for this test are: generator input signal at 31V, dwell time 43 μs, rise/fall time 5 μs, generation frequency at 300Hz, back pressure at -0.2inHg, strobe on time sets as 5 μs. The measured data are compared with literature data. Figure. 13 and Figure. 14 show the results of this repeatability analysis with surface tension and viscosity values compared for each data set. Standard deviation for surface tension and viscosity are estimated to be 1.138 and 0.057 respectively. The horizontal line shown in each figure represents the mean of reference values obtained from literature for this fuel. From Table 1, at 17°C, the mean surface tension from literature is 24.66 mN/m, and the mean viscosity from literature is 0.44 mPas.

4.d Surface tension and viscosity measurements

Figure. 15 and Figure. 16 show results for surface tension and viscosity obtained for the various biofuel candidates and two primary reference fuels (*n*-heptane and *iso*-octane) tested in this work. Candidate fuels from

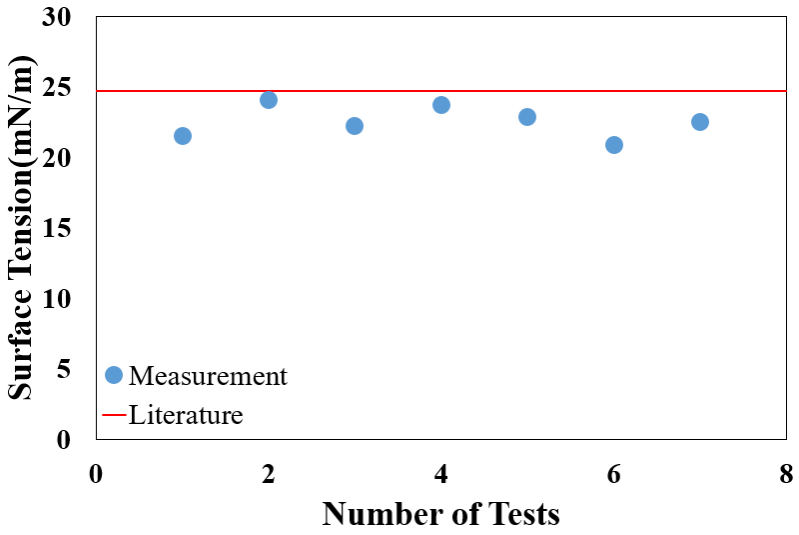

Figure. 13 Surface tension measurements for 2-Butanone repeatability analysis.

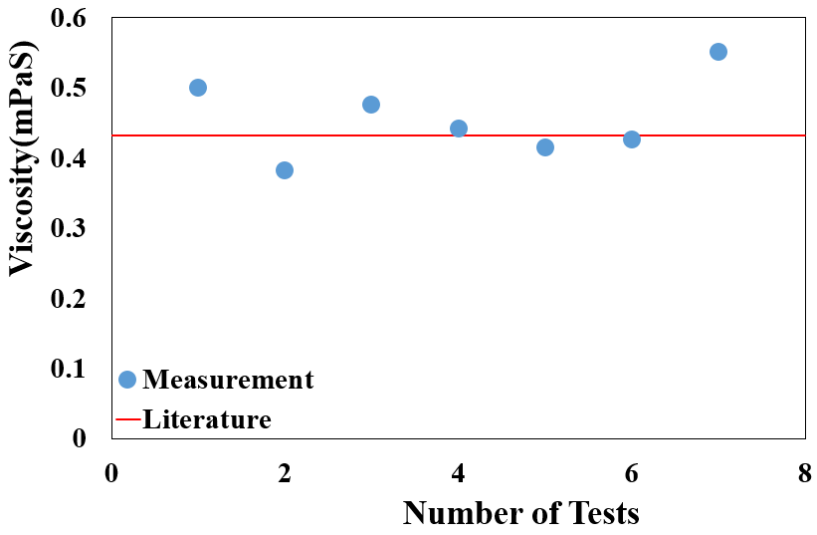

Figure. 14 Viscosity measurements for 2-Butanone repeatability analysis.

different functional groups have been selected including a furan, a ketone, an ester, and an alcohol. The results are compared with literature data [19-24] as well as measurements obtained using the reference instrument – tensiometer. The results from the measurement of droplet shape oscillation, reference measurement and literature data are close to each other. The most significant deviation in surface tension is observed for iso-octane, while that for viscosity is observed with 1-butanol. The measurements using droplet dynamics and using the reference instruments were carried out using identical fuel samples from the same source at the same ambient temperature. It is to be noted that the reference instrument measurements have uncertainties of the order of 8% in surface tension. Uncertainties are also associated with literature data. For the current measurements using droplet dynamics, it is imperative that a thorough uncertainty analysis be carried out while propagating errors starting from the imaging and image analysis techniques all the way to the equations used to estimate surface tension and viscosity using the oscillation amplitude decay curve.

This is part of ongoing work and will provide deeper insight into the deviation of the present results from published literature data. Reference instrument measurements using the viscometer will also be incorporated in future work.

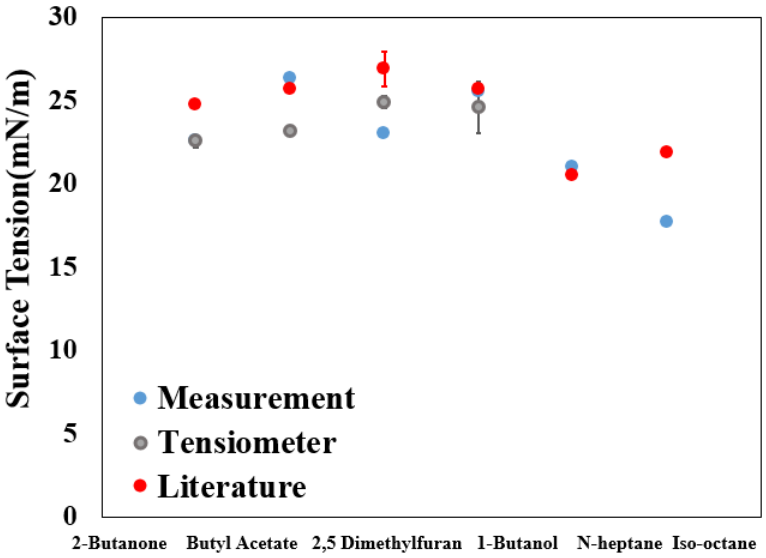

Figure. 15 Surface tension measurements for various candidate biofuels.

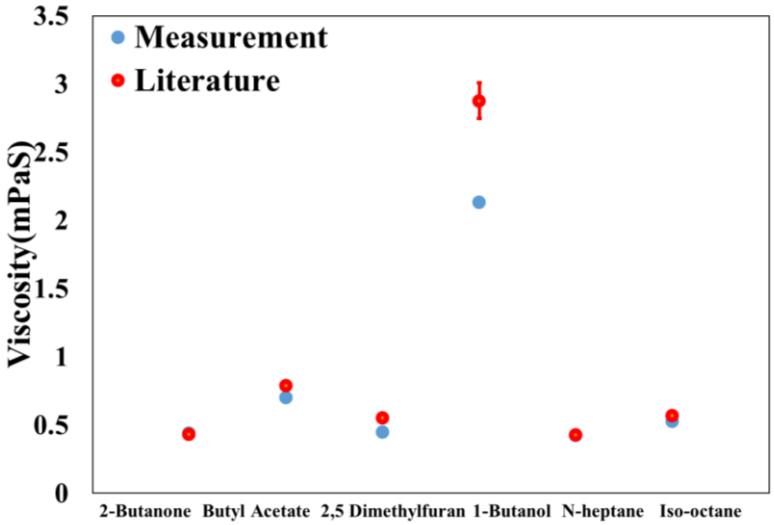

Figure. 16 Viscosity measurements for various candidate biofuels.

V. Conclusions

The utilization of biofuels as drop-in replacements for conventional fuels in internal combustion and gas turbine engines requires the evaluation of physical properties and combustion metrics of the fuels to ensure their compatibility with existing engines. Given the large number of candidate biofuels, it is desired to develop high-throughput screening techniques that can accomplish property evaluation using very small fuel samples. This work presents an approach to

measure fuel surface tension and viscosity of candidate biofuels using micro-liter quantities of the fuels using droplet dynamics. The oscillation of single droplets produced by a piezoelectric droplet generator is analyzed through hardware triggered stroboscopic imaging. Image processing and edge detection techniques are used to obtain the droplet radius as a function of polar angle during the course of its motion. The amplitude of oscillation is analyzed to obtain the decay rate as well as the eigenfrequency, which can be related to the fluid viscosity and surface tension. Measurements are obtained for primary reference fuels (*iso*-octane and *n*-heptane) as well as several candidate biofuel functional group molecules including alcohols, ketones, esters, and furans. Experimental results are compared with literature data as well as measurements obtained using reference instruments using standard ASTM procedures. Results show 0.4—19% deviation from average literature values for surface tension and 2—22% for viscosity. Repeatability tests conducted for one of the candidate biofuel molecules shows 2—15% deviation for surface tension and 0.5—25% deviation for viscosity from average literature values. A comparative study of edge detection algorithms showed the Prewitt operator to provide the best results given its equal weighting of pixels around the center of the droplet. Overall, given the present accuracy of the fuel surface tension and viscosity measurements, which use only about 5 µL of fuel and require about 500 µs per sample for data collection, show that the droplet dynamics based technique using a piezoelectric droplet generator provides a low-cost, high-throughput, small-volume fuel screening technique. Future work will focus on improvements in imaging through use of higher intensity light sources, expanding the study to higher pressures and temperatures of relevance to engine processes, and investigating heat of vaporization, which forms another key fuel physical property.

Acknowledgements

This research was conducted as part of the Co-Optimization of Fuels & Engines (Co-Optima) project sponsored by the U.S. Department of Energy (DOE) Office of Energy Efficiency and Renewable Energy (EERE), Bioenergy Technologies and Vehicle Technologies Offices. Nishir Mehta, Abid Hasan, Dr. Bhuvnesh Bharti, and Dr. Gartia from Department of Mechanical and Industrial Engineering, Louisiana State University provided the reference measurement using tensiometer and viscometer.

References

[1] Marsh, G. “Biofuels: aviation alternative?,” Renewable Energy Focus, 9(4), pp.48-51, 2008.
[2] Habib, Z., Parthasarathy, R., & Gollahalli, S., “Performance and emission characteristics of biofuel in a small-scale gas turbine engine,” Applied Energy, 87(5), pp.1701-1709, 2010.
[3] Bolszo, C. D., & McDonell, V. G., “Emissions optimization of a biodiesel fired gas turbine,” Proceedings of the Combustion Institute, 32(2), pp. 2949-2956, 2009.
[4] Mithun Das, Mouktik Sarkar, Amitava Datta, Apurba Kumar Santra., “Study on viscosity and surface tension properties of biodiesel-diesel blends and their effects on spray parameters for CI engines,” Fuel, Volume 220, 2018, pp. 769-779.
[5] Daniel P. Dupuis, R. Gary Grim, Eric Nelson, Eric C. D. Tan, Daniel A. Ruddy, Sergio Hernandez, Tyler Westover, Jesse E. Hensley, Daniel Carpenter., “High-Octane Gasoline from Biomass: Experimental, Economic, and Environmental Assessment.” Applied Energy Vol. 241 1 pp. 25-33, May 2019.
[6] Yalin Li, Shijie Leow, Tao Dong, Nicholas J. Nagle, Eric P. Knoshaug, Lieve M. L. Laurens, Philip T. Pienkos, Jeremy S. Guest, and Timothy J. Strathmann., “Demonstration and Evaluation of Hybrid Microalgae Aqueous Conversion Systems for Biofuel Production,” ACS Sustainable Chemistry & Engineering, 2019 7 (6), pp.5835-5844
DOI: 10.1021/acssuschemeng.8b05741
[7] Farrell, J., “Co-Optimization of Fuels and Engines (DOE/GO-102019-5150),” National Renewable Energy Lab.(NREL), Oak Ridge National Lab, Pacific Northwest National Laboratory, Sandia National Laboratories, 2018.
[8] Ling Tao, Jennifer N. Markham, Zia Haq, Mary J. Biddy., “Techno-economic analysis for upgrading the biomass-derived ethanol-to-jet blendstocks.” Green Chemistry Vol. 19 (4) 21 pp. 1082-1101, February 2017.
[9] Staat, H. J. et al.,”Ultrafast imaging method to measure surface tension and viscosity of inkjet-printed droplets in flight,” Experiments in fluids, 58(1), 2, 2017.
[10] Lamb H., *Hydrodynamics*, 6th ed., Cambridge University Press, Cambridge, 1932.
[11] N. Ashgriz., *Handbook of Atomization and Sprays*., Springer, pp. 125-134, 2011.
[12] Microfab, “Low temperature dispensing devices,” URL: http://www.microfab.com/images/pdfs/microjet_mf5.pdf
[13] Clyde E. Stauffer., “The Measurement of Surface Tension by the Pendant Drop Technique,” The Journal of Physical Chemistry 1965 69 (6), 1933-1938, doi: 10.1021/j100890a024

[14] J.M. Geist and M.R. Cannon., "Viscosities of Pure Hydrocarbons." Industrial & Engineering Chemistry Analytical Edition 1946 18 (10), 611-613, doi: 10.1021/i560158a008
[15] "Surface and interfacial tension and their measurement techniques," Biolin Scientific Technology Note 2 [online report],URL: https://cdn2.hubspot.net/hubfs/516902/Pdf/Attension/Tech%20Notes/AT-TN-02-Surface-and-interfacial-tension-techniques.pdf
[16] Cannon Instrument Company, "CANNON-Fenske Routine Viscometer,"
URL: https://www.cannoninstrument.com/en/product/manual-glass-viscometers
[17] Ramesh Jain, Rangachar Kasturi, and Brian G. Schunck., *Machine Vision*. McGraw-Hill, Inc, New York, NY, pp. 140-185, 1995.
[18] Trujillo-Pino, A., Krissian, K., Alemán-Flores, M., & Santana-Cedrés, D. "Accurate subpixel edge location based on partial area effect," Image and Vision Computing, 31(1), pp. 72-90, 2013.
[19] Haynes, W. M., Lide, D. R., & Bruno, T. J., *CRC handbook of chemistry and physics: a ready-reference book of chemical and physical data*, 97th Edition, CRC Press, Boca Raton, Florida, 2016.
[20] Carl L. Yaws., *Thermophysical Properties of Chemicals and Hydrocarbons*. William Andrews Publishing, 2008.
[21] Ming Jer Lee and Ming Chi Wei.,"Densities and viscosities of 2-butanone/dibutyl ether, 2-picoline/2-butanone, and 2-picoline/water mixtures," Journal of Chemical & Engineering Data, 1992 37 (2), pp. 209-212, doi: 10.1021/je00006a019.
[22] Julio Lopes da Silva, Martín Aznar., "Thermophysical properties of 2,5-dimethylfuran and liquid–liquid equilibria of ternary systems water+2,5-dimethylfuran+alcohols (1-butanol or 2-butanol or 1-hexanol)," Fuel, Volume 136, 2014, pp. 316-325, URL: https://doi.org/10.1016/j.fuel.2014.07.039 .
[23] Coker AK, Ludwig EE., *Ludwig's Applied Process Design for Chemical and Petrochemical Plants*. [Electronic Resource]. URL:https://search-ebscohost-com.libezp.lib.lsu.edu/login.aspx?direct=true&db=cat00252a&AN=lalu.2767381&site=eds-live&scope=site [Retrieved July 11, 2019]
[24] Mejía A, Segura H, Cartés M. "Isobaric vapor-liquid equilibrium and isothermal interfacial tensions for the system ethanol + 2,5-dimethylfuran," J Chem Eng Data, 58:3226–32, 2013.